Egypt. J. Chem. **Vol. 65**, No. 5 pp. 623 - 633 (2022)

Egyptian Journal of Chemistry

http://ejchem.journals.ekb.eg/

Studies on Electrodeposition of Zinc Selenide and Zinc Telluride and Their Photoelectrochemical Cell Behavior

Elsayed Mostafa Elsayed,[1*] and Atef Yousef Shenouda[1]

Chemical and ElectroProcessing Division, Mineral Technology Department, Central Metallurgical Research & Development Institute, P.O.Box 87Helwan, 11421, Egypt

Abstract

The electrochemical behavior of Zn2+, Se4+ and Te4+ ions was investigated using cyclic voltammetry measurements. The electrodeposition of zinc selenide (ZnSe) and zinc telluride (ZnTe) was conducted on titanium sheet substrates using the potentiostatic technique.The electrodeposition of zinc selenide occurred at a potential of -0.5 V while zinc telluride was deposited at a potential of -0.7 V using mercuric-mercurios sulphate electrode (MSE; Hg/ Hg2SO4/ H2SO4) as reference electrode. The X-Ray Diffraction (XRD) data revealed that, the characteristic peaks of the cubic system structure for and zinc selenide and zinc telluride are formed with well cubic structural phases. The transmission is measured by UV-VIS-NIR spectrophotometer. The transmission edge observed during the UV-VIS-NIR spectra measurement occurred at 660 nm for the electrodeposited ZnSe, while the transmission of ZnTe occurred at 750 nm. In addition, the efficiencies of the photoelectrochemical solar cells are 5.1% and 7.1% for ZnSe and ZnTe, and the energy gap values are well detected at 2.5 and 2.27 eV for ZnSe and ZnTe, respectively. The electrochemical impedance spectra showed that zinc telluride is more conductive than the zinc selenide.

Keywords: ZnSe, ZnTe, Electrodeposition, Photoelectrochemical cells, Electrochemical measurements

1. Introduction

The II–VI compound semiconductors have recently brought significant concern due to their new physical properties and their implementations in many of optoelectronic instruments [1–7]. In group II-VI, ZnSe has received particular attention, and it has come to the fore with the advent of high efficiency photovoltaic cells and short wavelength light emitters. Zinc selenide (ZnSe), in cubic blend structure of Zn, has a value of direct band gap energy around 2.7eV at 25 ^{0}C. Therefore, it has a wide range of applications in instruments such as blue light-emitting diodes [8, 9],photodiodes [10], thin film transistors [11, 12], and Cr doped ZnSe laser [13, 14]. In addition, it has been served as an alternative material rather than cadmium selenide in solar cells containing Cu (In, Ga)Se2 (CIGS) [15, 16]. Cadmium plating and cadmium sulphid have many important applications in industry [17–19] . It is worth noting that Zinc selenide has numerous benefits over its predominant competitor CdS, including lower toxicity, wider band gap and a better lattice compared with the copper–indium–gallium–diselenide (CIGS) absorber layer. Bula et al [20] performed ZnSe thin film layers of different thickness on glass substrate at temperature of 150 °C. The X-Ray pattern indicated the formation of a cubic structure with orientation in (111) direction. The grain sizes increased and the crystallinity was improved with the increase of the film thickness. On the other hand, the band gap energy value decreased from 2.92 to 2.69 eV with increasing the film thickness [21–24]. The mechanisms of Zn, Se and ZnSe deposition were investigated [25]. Chronoamperometry and cyclic voltammetry techniques were compared to quartz crystal microbalance technique to analyze the deposition. Both techniques have a significant impact on the applied potentials. Pure selenium (Se) was electrodeposited at zero volte versus saturated

*Corresponding author e-mail: elsayed2021@gmail.com
Receive Date: 12 October 2021, Revise Date: 04 November 2021, Accept Date: 09 November 2021
DOI: 10.21608/EJCHEM.2021.100720.4679

calomel electrode. After that, H2Se was formed and it reduced the current efficiency value. Moreover, the current efficiency decreased with increasing the electrode potential in its negative value. This was attributed to the evolution of hydrogen gas (as a side reaction) and the formation of H2Se. Voltammetric and microgravimeteric results indicated that Zn electrodeposition from electrolyte, in presence of ions followed with deposition of Se to prepare ZnSe deposition, were started at -0.6 V versus SCE. The The chronoamperometric transients combined with microgravimetry confirmed the range of potentials in which ZnSe and Se were deposited. The H2Se was existed with a potential lower than -0.8 versus SCE. After that, it was combined with Zn2+ cations demonstarated electro deposition mechanism for ZnSe. On the other hand, for ZnTe electrodeposition, polycrystalline ZnTe films were created by electrochemical deposition onto semiconductor and metallic electrodes using an acidic bath. Zinc blend mixes containing polycrystalline ZnTe films have been created [26, 27]. The microstructure was obtained and evaluated by electrodepositing from an acidic sulphate bath using pulsating current in terms of stoichiometry and crystallinity. Also, the microstructure was improved in presence of citrate ligand where uniform and smooth films of ZnTe were formed. It was stated that, the deposited film may contain citrate species that can be co-deposited and involved as impurities in the deposited ZnTe films. In addition, the growth of the ZnTe film was accompanied by vigorous electrode influences. The electrodeposition of ZnTe films (Electrochemical-Atomic Layer Deposition) on the carboxyl-functionalized multi-walled carbon nanotubes / polyimide (COOH-MWCNTs/PI) membrane was also reported [28]. The crystal growth mechanism of the prepared ZnTe film was discussed. The structure of the deposited film was strongly affected by the deposition cycle and reagent concentration. The direct band gap energy was 2.26 eV based on UV-visible transmission data. The conductivity of p-type ZnTe dendritic film was evinced by photoelectrically data. These specified that the prepared ZnTe film had a useful use in optoelectronic instruments. The present work focused on electro deposition of ZnTe and ZnSe using various lower and higher Te4+ and Se4+ compositions in order to achieve suitable electrocodeposition and photoelectrochemical cell performance. The aim of this work is to study the effect of different Se4+ and Te4+ ion concentrations on the deposition potential of ZnSe and ZnTe. In addition, the effect of the electrochemical behavior of electrodeposited ZnSe and ZnTe films in relation to the solar cell parameters of the photo electrochemical cells was investigated and thoroughly addressed.

2. Experimental

2.1. Electrochemical measurements

Cyclic voltammetric and potentiostatic studies were performed and recorded using a computer controlled potentiostat (Volta lab 21 with voltamaster software) PGP 201 Potentiostat, France. Prior to carry out the experiments, the platinum and titanium electrodes were cleaned before electrodeposition in ultrasonic bath with acetone, ethanol and ultrapure de-ionized (DI) water for 20 min, respectively. Solutions were adjusted to pH 2.5 by adding dilute reagent grade sulfuric acid and ammonia solution (NH4OH). The temperature was maintained at 25 °C. All solutions were freshly prepared prior to perform each experiment.

2.1.1. Cyclic voltammetry measurements

Zinc sulphate (ZnSO4.7H2O, 99%, Loba Chemie, India) and SeO2 (99%, Loba Chemie, India) or TeCl4 (99.9%, Strem, USA) were dissolved in ultrapure de-ionized (DI) water with magnetic stirring. Cyclic voltammetric (CV) study for ZnTe was carried out using different TeCl4 concentrations: 1, 2, 3, 4 and 5 mM Te4+ that mixed separately with 0.1 M Zn2+ to form the bath solutions. Also, the CV studies of ZnSe were carried out on bath solutions containing: 0.1 M Zn2+ mixed separately with different SeO2 concentrations: 1, 1.5, 2, 2.5, 3, 3.5, and 4 mM Se4+. The working electrode was Pt rotating disc electrode of 3 mm diameter (RDE, Model EG and G Electro-instrument, USA). The counter electrode was Pt wire electrode of 2 mm diameter. All potentials were measured with respect to saturated Mercuric-mercurios sulphate reference electrode MSE (Hg/ Hg2SO4/ H_2SO_4). A potential range between 0 and -1.8 V with a scan rate 5 mVs-1 was used. We started scanning directly from 0 V to -1.8 V upon that cathodic side, then swapped onto anodic side.

2.1.2. Potentiostatic measurements

In another series of experiments, ZnSe and ZnTe films were deposited on titanium sheet cathodes using potentiostatic technique. The potentiostatic electrodeposition was run for ZnSe at -0.5 V and for ZnTe at -0.7 V versus MSE using a titanium

sheet substrate with exposed area 4 cm2. The studied baths concentrations were 0.1 M Zn2+ with 3 mM Se4+ and 0.1 M Zn2+ with 4 mM Te4+ . Platinum sheet was used as counter electrode with the previous potentiostat (Volta lab). The electrodeposition was carried out for about 45 minutes in order to obtain a suitable yield from each compound. For optical measurements, ZnSe or ZnTe was electrodeposited on indium tin oxide (ITO) conducting glass slide of dimensions 7.5 cm x 2.5 cm x 1.1 mm. The electrodeposition was performed under the same experimental potentiostatic conditions for 30 min. The electrode area was coated with ZnSe or ZnTe was 4 cm x 2.5 cm.

2.2. ZnSe and ZnTe characterization and optical measurements

The coated electrodeposited ZnSe and ZnTe samples were taken from the Ti-substrate as powder. The crystal structures were studied using Powder X-ray diffraction (XRD). The XRD investigations were carried out using a Brucker axis D 8 diffractometer with crystallographic data software Topas 2 using Cu-Kα (λ= 1.5406 A) radiation operating at 40 kV and 30 mA. Scanning electron microscopy (SEM) a JEOL SEM Model 5040 was used for morphological investigation. Optical measurements for the transmission and absorption spectra were carried out by using spectrometer JASCO Corp., V-570. The conducting ITO glass slide coated with either ZnSe or ZnTe was used in the housing holder versus ITO one as a blank.

2.3. Photoelectrochemical and electrochemical impedance spectra (EIS) measurements

The electrodeposition of ZnSe and ZnTe on titanium electrode was executed using photochemical cell. Titanium plate was used as a cathode and the Pt electrode worked as an anode. The cell configuration was Ti: ZnSe or ZnTe/0.5 M Na2S + 0.5 M S + 0.5 M NaOH/Pt. It is used for electrochemical impedance spectra (EIS) and current–voltage (I–V) characteristics measurements [29]. For EIS measurements [30], the amplitude signal was 10 mV and the frequency changed from 1 M Hz to 10 m Hz using Potentiostat (Parastat 4000, Princeton, USA). The photo-electrochemical cell experiments were performed by using solar simulator Sciencetech SS150W- AAA. The cell was exposed to light intensity 1 Sun (100 mW/cm2) using Air Mass 1.5 Global Filter. The I-V tester was 2400 Keithley source. The solar cell parameters (V_{OC}, I_{SC}, P_{mp}, FF and η) were accordingly recorded.

3. Results and Discussions

3.1. Electrochemical behavior of ZnSe and ZnTe

The potentiodynamic measurement of 0.1 M Zn^{2+} + 1- 4 mM Se^{4+} (SeO_2) ions at pH= 2.5 and 25 °C is shown in Fig.1. It is noticed that the optimum concentration of Se^{4+} ions was 3 mM where a higher deposition current was observed at -4.4 $mAcm^{-2}$ (Fig. 1)

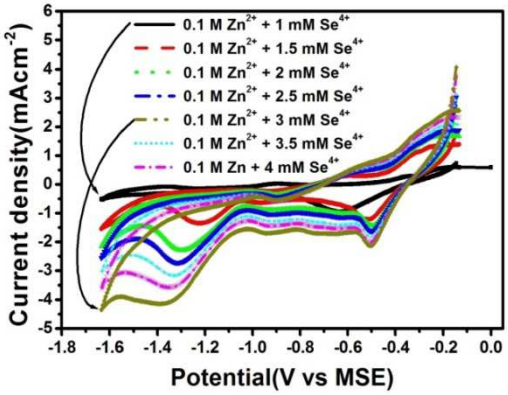

Fig.1 Cyclic voltammograms of solution containing 0.1 M ZnSO4 + 1- 4 mM Se at pH =2.5

The cathodic electrodeposition of ZnSe was observed at a potential -0.5 V versus MSE. Moreover, potentiodynamic measurements of 0.1 M Zn + 3 mM Se in comparison with 0.1 M Zn and 3 mM Se were achieved (Fig.2.) Cyclic voltammogram shows a very low deposition current of -0.5 mA cm^{-2} with 3 mM Se while a current of -1.2 $mAcm^{-2}$ was recorded with cyclic voltammogram of 0.1 M Zn^{2+} ion bath. The cyclic voltammogram of 0.1 M Zn + 3 mM Se showed better behavior and provided higher electrodeposition current than that of cyclic voltammogram of Zn or Se ion itself (-4.4 $mAcm^{-2}$). On reversing the scanning in anodic direction, the anodic dissolution of ZnSe was noticed at a potential of -0.19 V.

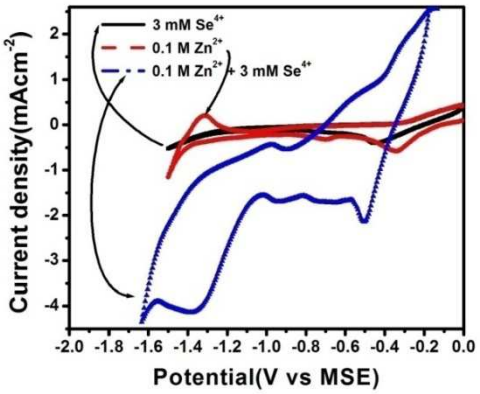

Fig. 2 Cyclic voltammograms of solution containing 3 mM Se^{4+}, 0.1 M Zn^{2+} , 0.1 M Zn^{2+} + 3 mM Se^{4+} at pH =2.5

The potentiodynamic measurements of 0.1 M Zn^{2+} + 1 to 5 mM Te^{4+} ions are shown in Fig. 3. Electrodeposition of ZnTe film occurred at potential -0.7 V versus MSE for a bath containing 0.1 M Zn^{2+} with 2, 3 and 5 mM Te^{4+} ions. Furthermore, the anodic dissolution for ZnTe was executed at potential of - 0.245 V.

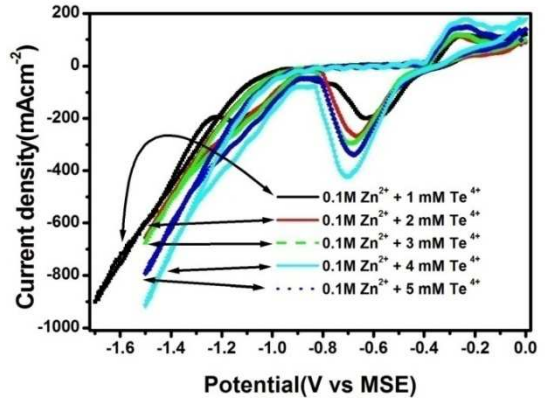

Fig. 3 Cyclic voltammograms of solution containing 0.1 M Zn^{2+} + 1-5 mM $TeCl_4$ at pH = 2.5

According to available data in Figure 1,2,3, the potentials -0.5 and -0.7 V vs. MSE for ZnSe and ZnTe are derived from the best conditions of potentiodynamic measurements of Zn^{2+}, Se^{4+}, and Te^{4+} ions bath solutions.

The change in current density with time for ZnSe electrodeposited on Ti electrode in a bath containing 0.1 M Zn^{2+} + 3 mM Se^{4+} ions for 45 minutes at a pH value of 2.5 is shown in Fig. 4.

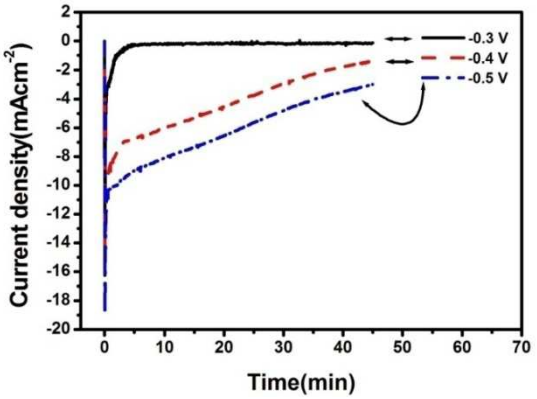

Fig. 4 *I-t* potentiostatic curves for deposition of ZnSe from 0.1 M Zn^{2+} + 3 m M Se^{4+} at constant potentials using Ti cathode

The progress of current density curves as a function of time was similar for all of the tested potentials -0.3, -0.4, and -0.5 V. The current sharply increased with passing the deposition potential at first 60 s (Fig. 4). This is most probably due to the start of crystal nucleation and the development of each crystal increased through the area of the Ti cathode. Increasing the deposition time over 60 s causes a decrease in current density because all ions in the electrical double layer adjacent to the cathode are deposited. The current time transient curves can be separated into three regions:- the first region corresponding to short times (time < 0.5 s). In this region, the current quickly increases and sharply rises with passing the deposition potential (Fig. 4). The second region related to the crystal nucleation process and growth of the crystal formed during the first region (> 80 s). The third region related to the decline in the current density, which represented the diffusion progress, where, the ions start to migrate from the bulk to the cathode surface in steady state migration. More deposition time (> 600 s) results in a leveling of deposition current values with a steady state plateau (Fig. 4). After that, the progress of current with time shows three-dimensional nucleation and development of crystals in three dimensional growths [31]. Furthermore, the behaviour of the nucleation process is controlled by the value of applied potential. The recorded current density plateau increased with increasing the applied potential. The recorded current values were -1 mA cm^{-2} at potential value of -0.3 V, -2 $mAcm^{-2}$ at a potential value of -0.4 V, and 4 $mAcm^{-2}$ at a potential value of - 0.5 V. Furthermore, the effect of constant deposition potential on the electrodeposited ZnTe compound deposited from a solution containing 0.1 M Zn^{2+} + 4 mM Te^{4+} ions is

shown in Figure 5. Potentiostatic measurements were performed for 45 min at various potentials mainly -0.3, -0.4, -0.5 and -0.7 V at pH 2.5.

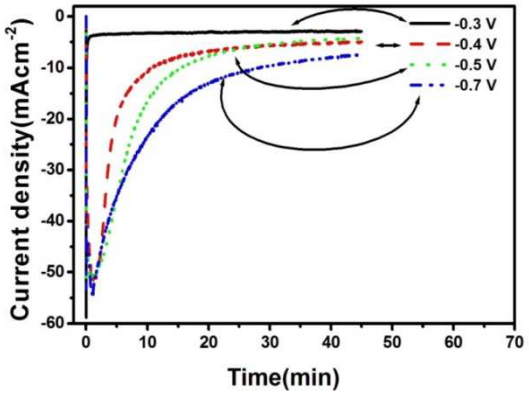

Fig. 5 *I-t* potentiostatic curves for deposition of ZnTe from 0.1 M Zn^{2+} + 3 m M Te^{4+} at constant potentials using Ti cathode

The current density versus time curves for ZnTe layers electrodeposited on Ti electrode is displayed in Fig. 5. The current density curves are similar in their progress with time for all tested potentials. The current densities sharply increased with the first few seconds of passing the deposition potential (at first 60 s). The crystal nucleation started and the deposited crystals increased the area of the Ti cathode (Fig.5). ZnTe, as interpreted with ZnSe, has a similar rationale for increasing the time, three-dimensional nucleation, and growth of crystals. The recorded current values were -4 $mAcm^{-2}$ at potential of-0.3 V, -7 $mAcm^{-2}$ at -0.4 V, -7.1 at -0.5 V, and -9 $mAcm^{-2}$ at -0.7 V (Fig. 5).

3.2. XRD characterization

Fig 6 depicts the XRD patterns for a deposited ZnSe and ZnTe powder. The pattern of ZnSe shows one intense and four diffraction peaks at 2θ values of approximately 27, 45, 54, and 66.5°, corresponding to the crystal planes of (111), (220), (311), and (331), respectively. They are typical diffraction peaks of cubic for ZnSe with JCPDC data (No. 01-6920). The obtained XRD pattern peaks are in good agreement with those reported literature [25]. The XRD of the deposited ZnTe film using 0.1 M Zn^{2+} + 4 mM Te^{4+} is shown in Fig.6 (b).

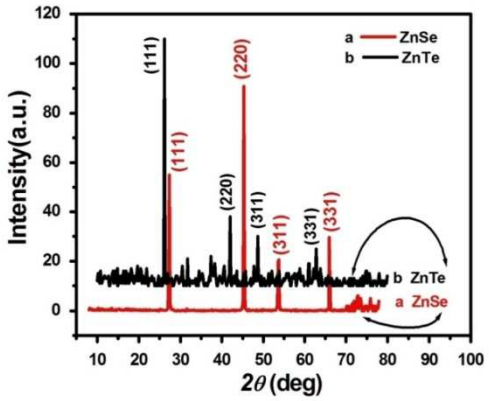

Fig. 6 XRD patterns of (a) ZnSe film electrodeposited from solution containing 0.1 M Zn + 3 mM Se at -0.5 V (b) ZnTe film electrodeposited from solution containing 0.1 M Zn - 4 m M Te at -0.7 V

It exhibit main diffraction peaks at 2θ positions of 26, 42, 51, and 63°, which refer to the crystal planes of (111), (220), (311), and (331), respectively. The sharp peaks of the sample indicate the good crystallinity of the deposited films. The peaks have the miller indices that match with the cubic ZnTe planes and it is confirmed with JCPDC data (19-0191) of ZnTe planes. This XRD data agrees with the previous reports [20, 28]. The crystallite sizes of ZnSe and ZnTe samples are calculated using Scherer equation [32]:

$$D = 0.9\lambda/(\beta\cos\theta) \qquad (1)$$

where λ is the wavelength (λ = 1.5418 A) ($Cu_{K\alpha}$), β is the full width at the half-maximum of the line and θ is the diffraction angle in radian scale. The obtained values are 93.9 and 38.1 nm for ZnSe and ZnTe samples, respectively. So, ZnTe has more nano-crystalline structure than ZnSe. Also, the average micro strain (ε) is given by:

$\varepsilon = \beta \cot \theta / 4$ (2)

The micro strain values are 3.85 x 10^{-4} and 9.5 x 10^{-4} for ZnSe and ZnTe samples, respectively. Obviously, the obtained values of crystallite size and micro-strain show an inverse relationship between ε and D, which could be attributed to the decrease in the volume occupied by the constituents inside the crystalline structure [32].

Therefore, ZnTe has lower crystallite size and higher lattice strain than ZnSe. It is worth mentioning here that strain effects originate from a systematic shift of the atoms from their ideal positions as a result of point defects, dislocations, and vacancies in the crystal structure [33].

3.3. SEM Investigation

The SEM micrograph of electrodeposited ZnSe powder prepared from solution containing 0.1 M Zn^{2+} + 3 mM Se^{4+} using potentiostatic conditions is shown in Fig 7a. The average particle size of electrodeposited ZnSe is about 2 µm. Fig.7b shows the SEM of potentiostatic electrodeposited ZnTe powder prepared from a solution containing 0.1 M Zn^{2+} + 4 mM Te^{4+}. The average crystal size is about 200 nm. So, ZnTe has a particle size smaller than ZnSe

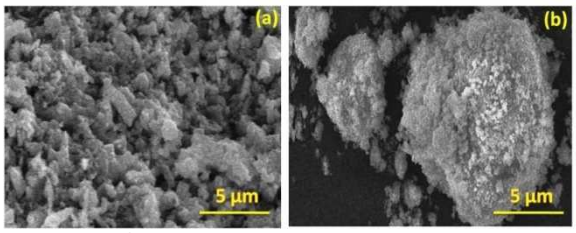

Fig. 7 SEM of electrochemically deposited (a) ZnSe and (b) ZnTe

3.4. Transmission spectra

The transmission spectra of electrodeposited ZnSe and ZnTe films on ITO are depicted in Fig.8a, b.

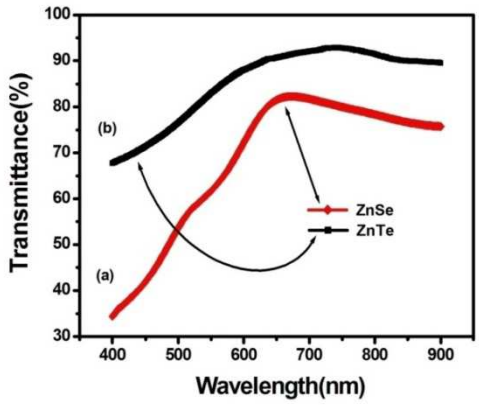

Fig. 8 Transmission spectra of electrodeposited (a) ZnSe (b) ZnTe

The onset of electro of transmission occurred at 660 nm for electrodeposited ZnSe (Fig. 8a), while the transmission of ZnTe is detected at 750 nm (Fig.8b). For a direct band gap material, the energy band gap is calculated using the relation between $(\alpha h\nu)^2$ and the photon energy $h\nu$ (Fig.9a,b).

band gap is calculated using the relation between $(\alpha h\nu)^2$ and the photon energy $h\nu$ (Fig.9a,b).

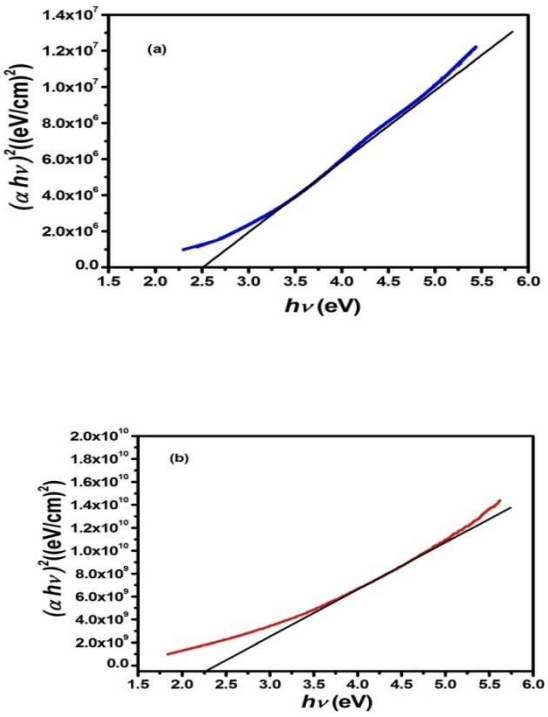

Fig. 9 Tauc plot for electrodeposited (a) ZnSe and (b) ZnTe

The coefficient of absorption "α" is given by equations 3-5 [34–36].

$$log\ (1 / T) = \alpha t\ / 2.303 \quad (3)$$

$$A = log\ (I / I°) = \alpha t / 2.303 \quad (4)$$

A is the Absorbance. *t* is the thickness of the resulting film, and *T* represents the spectral transmittance. The *I*° and *I* are intensities of both incident and transmitted light inside the tested sample. The coefficient of absorption (α) can be calculated for direct band transition by the following equation:

$$\alpha h\nu = B\ (h\nu - E_g)^{0.5} \quad (5)$$

The value of band gap energy (E_g) can be obtained by extrapolation in Fig 9 a,b. The symbol *B* in equation 5 is a constant, which is called the band tailing parameter and it is an energy independent constant [34]. The value of E_g is expected to be between 2.5 eV for ZnSe and 2.27eV for ZnTe films on ITO, respectively [28, 37].

3.5. *I-V* and *EIS* Characteristics

The electrochemical impedance spectra of electrodeposited ZnSe and ZnTe are shown in Fig. 10. It is observed that the ZnTe cell has a bulk resistance cell of about 2000 Ω, while the ZnSe has a value of 5250 Ω. Therefore, ZnTe is more conductive than ZnSe.

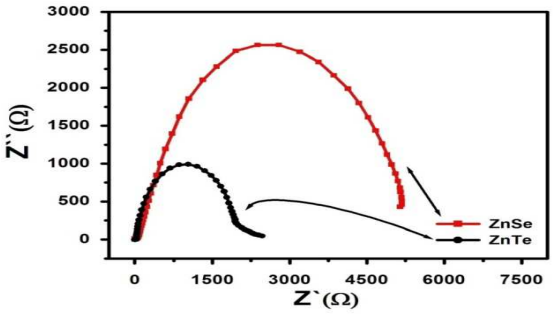

Fig. 10 *EIS* of ZnSe and ZnTe electrochemical cells

To get the solar cell parameters, the illumination of the photoelectrochemical cell (*PEC*) was set at 100 mW/cm^2. The open circuit potential (V_{oc}) was recorded for the deposited ZnSe and ZnTe films. Also, the short circuit currents (I_{sc}) were recorded for the same deposited film (Table 1).

The current-voltage (*I-V*) curves and the output results of photoelectrochemical ZnSe and ZnTe films are shown in Fig.11.

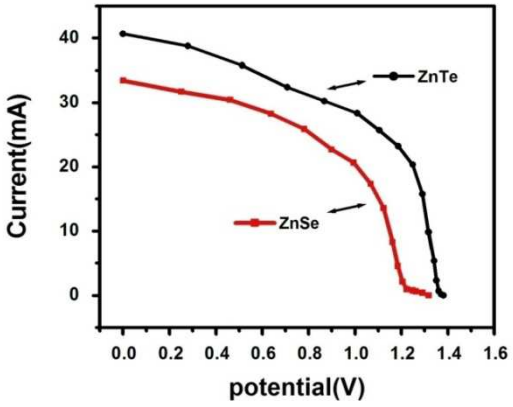

Fig. 11 Current-potential characteristics of ZnSe electrochemical cell and ZnTe electrochemical cell under illumination

These results are analyzed to give fill factor (*FF*) and conversion efficiency (η%) as represented by equations 6 and 7 and listed in Table 1. The data revealed that the I_{sc} of the deposited ZnTe is higher than ZnSe. The efficiency of photo-conversion per unit area is 7.09% and results using simple conditions with the deposited ZnTe films while, 5.1% is obtained for ZnSe films (Table1).

$$FF = V_{mp} I_{mp} / V_{oc} I_{sc} \quad (6)$$

$$\eta = (V_{mp} I_{mp} / P_{in} * A) * 100 \quad (7)$$

Where, I_{mp} is the maximum power point current and V_{mp} is the maximum power point voltage. There is an important factor that the photoelectrochemical cell has lower efficiency than the photovoltaic cell as the incident light drops vertically on the cell and not perpendicularly. This allows for the loss of some power. Furthermore, the electrolyte separation is considered as a kind of barrier between the photo anode and the photo cathode electrodes that wastes the energy of the incident light, while the photovoltaic has thin films based on using thinner semiconductor layers to

absorb and convert sunlight. For example, CdTe photovoltaic cell efficiency is approaching 20% in the laboratory with a record of 22.1% in 2016 [38],while CdTe photoelectrochemical cell efficiency is 1.12% as reported in the literature [35].

Table 1: Photo electrochemical cell (*PEC*) parameters for ZnSe and ZnTe electrodeposited on titanium substrate

Deposited compound	V_{oc} [V]	I_{sc}[mA]	V_{mp} [V]	I_{mp}[m A]	*FF*[%]	η[%]
ZnSe	**1.31**	**33.4**	**0.90**	**22.68**	**46.3**	**5.1**
ZnTe	**1.38**	**40.7**	**1.11**	**25.67**	**50.6**	**7.1**

4. Conclusions

Electrodeposition of ZnSe and ZnTe thin films was studied using cyclic voltammeteric and potentiostatic techniques**.** The cathodic deposition of electrodeposited ZnSe was carried out at potentials -0.3, -0.4 and -0.5 V versus MSE. The cyclic voltammogram of 0.1 M Zn + 3 mM Se showed better performance than that of Zn or Se ion itself. The cyclic voltammogram and anodic dissolution of ZnSe occurred at potential -0.19 V. The cathodic deposition of ZnTe film occurred at -0.7 V versus MSE for a bath containing 0.1 M Zn^{2+} + 4 mM Te^{4+} ions. Potentiostatic studies were performed for the cathodic deposition of ZnSe and ZnTe at different potentials from solutions containing 0.1 M Zn^{2+} + 3 mM Se^{4+} ions and 0.1 M Zn^{2+} + 4 mM Te^{4+} ions. The deposition current densities of ZnSe and ZnTe films increased with increasing the applied potentials. The XRD patterns illustrated that the electrodeposited ZnTe and ZnSe powders are cubic structures.

The average particle size of electrodeposited ZnSe is 2 µm, while the average particle size of ZnTe is 200 nm. The onset of― transmission spectra occurred at 660 nm for the electrodeposited ZnSe while it was 750 nm for ZnTe. The energy gap (E_g) was 2.5 eV for ZnSe and 2.27 eV for ZnTe. The efficiency of photo-conversion per unit area was 5.1% with electrodeposited ZnSe films and 7.1% with ZnTe films. The electrochemical impedance spectra indicated that the electrodeposited ZnTe is more conductive than ZnSe. For companies that develop blue light-emitting diodes, photodiodes, and thin film transistors, this research work is very important.

5. Acknowledgment

The authors would like to thank Science, Technology and Development Fund (STDF) for financial support of this study through the joint project No 421 of Egypt-US A. Also, the authors would like to express our deepest thanks to Prof. Dr. Lee Chow, Department of Physics, University of Central Florida, Orlando, Florida 32816, USA for his comments and suggestions.

6. References

1. Kumar T. R., Growth of ZnSe by electrochemical deposition method. *International Journal of Pure and Applied Mathematics***, 119**, 2657–2666(2018).
2. Sharma Y.C., Ansari P., Sharma R., Mathur D. and Dar R.A., Bandgap tuning of optical and electrical properties of zinc selenide. *Chalcogenide Letters* **18**, 183–189(2021).
3. Chaure N.B. and Chaure S., Investigation on the effect of Cu-doping to ZnTe layers by low-cost electrochemical approach. *Journal of Materials Science: Materials in Electronics*, **28**, 11823–11831(2017).https://doi.org/10.1007/s10854-017-6990-7
4. Babatunde R.A., Odunaike R.K., Talabi A.T. and Taofiqadeleke, A., Synthesis and characterization of ZnSe thin films deposited by thermal vacuum evaporation method for photovoltaic application. *Applied Journal of Environmental Engineering Science*, **3**, 227–237 (2020).
5. Omarova A., Kadyrzhanov K., Kozlovskiy A., Kaniukov E. and Zdorovets M., Study of the

influence of synthesis conditions on stoichiometry and the properties of nanostructured CdSe thin films. *Journal of Materials Science: Materials in Electronics*,**31**, 12756–12764(2020). https://doi.org/10.1007/s10854-020-03827-4.

6. Singh H., Duklan N., Singh T., Thakur A. and Sharma J., Effect of vacuum annealing on structural and optical properties of nanocrystalline ZnTe thin films. *Journal of Materials Science: Materials in Electronics*, **29**, 4992–4998(2018). https://doi.org/10.1007/s10854-017-8460-7.
7. Omarova A., Kadyrzhanov K.K., Giniyatova S.G., Kozlovskiy A.L. and Zdorovets M. V., Study of structural and morphological features of nanostructured coatings based on CoCdSe. *Solid State Sciences*,**106**, 106339(2020). https://doi.org/10.1016/j.*solidstatesciences*.2020 .106339
8. Won Y., Cho O., Kim T., Chung D., Kim T., Chung H., Jang H., Lee J., Kim D. and Jang E., Highly efficient and stable InP / ZnSe / ZnS quantum dot light-emitting diodes. *Nature*, **575**, 634–638 (2019). https://doi.org/10.1038/s41586-019-1771-5.
9. Dmitruk I., Berezovska N., Degoda V., Hrabovskyi Y., Kolodka R., Podust G., Stanovyi O. and Blonskyi I., Luminescence of Femtosecond Laser-Processed ZnSe Crystal. *Journal of Nanomaterials*, **2021**, 1–9(2021). https://doi.org/10.1155/2021/6683040.
10. Rao G.K., Electrical and photoresponse properties of vacuum deposited Si / Al : ZnSe and Bi : ZnTe / Al : ZnSe photodiodes. *Applied Physics A*, **123**, 1–9(2017). https://doi.org/10.1007/s00339-017-0850-4
11. Al Garni S.E. and Qasrawi A.F.,Absorption and optical conduction in InSe/ZnSe/InSe thin film transistors. *Functional Materials Letters*, **9**, 1650019(2016).
12. Al Garni S.E. and Qasrawi A.F., Impedance spectroscopic analysis of the InSe/ZnSe/InSe interface. *IEEE Transactions on Electron Devices*, **64**, 244–249(2017). https://doi.org/10.1109/TED.2016.2623649
13. Parks J.U.R.S., Ro S.T.C.A., Ongrui R.H.E., Oetz M.E.L.G., Rug J.A.P.K., Aniel S.E.A.N.A.M.C.D., Erry P.A.A.B., Ook G.A.R.Y.C., Chepler K.E.L.S., Azio P.I.E.R.J.S., Opalan V.E.G. and Ohn J. V, Chromium doped zinc selenide optical fiber lasers. *Optical Materials Express*, **10**, 1843–1852(2020).
14. Asilyev S.E. V, Oskalev I.G.O.R.M., Irov M.I.K.E.M., Molski V.I.S., Irov S.E.M. and Apontsev V.A.G., Ultrafast middle-IR lasers and amplifiers based on polycrystalline Cr : ZnS and Cr : ZnSe. *Optical Materials Express*, **7**, 2636–2650(2017).
15. Chuhadiya S., Sharma R., Patel S.L., Chander S., Kannan M.D. and Dhaka M.S., Physica E : Low-dimensional Systems and Nanostructures Thermal annealing induced physical properties of ZnSe thin films for buffer layer in solar cells. *Physica E: Low – dimensional systems and Nanostructures*. **117**, 113845(2020). https://doi.org/10.1016/j.physe.2019.113845.
16. Soonmin H.O., Power conversion efficiency in thin film solar cell : A review. *International Journal of Chemical Sciences*, **14**, 143–151(2016).
17. Reda Y., El-Shamy A.M. and Eessaa A.K., Effect of hydrogen embrittlement on the microstructures of electroplated steel alloy 4130. *Ain Shams Engineering Journal*, **9**, 2973–2982(2018). https://doi.org/10.1016/j.asej.2018.08.004.
18. Reda Y., El-Shamy A.M., Zohdy K.M. and Eessaa A.K., Instrument of chloride ions on the pitting corrosion of electroplated steel alloy 4130. *Ain Shams Engineering Journal*, **11**, 191–199 (2020). https://doi.org/10.1016/j.asej.2019.09.002
19. El-Shamy A.M., Reda Y., Zohdy K.M. and Eessaa A.K., Effect of plating materials on the corrosion properties of steel alloy 4130. *Egyptian Journal of Chemistry*, **63**, 579–597(2020).https://doi.org/10.21608/ejchem.2019 .11023.1706

20. Balu A.R., Nagarethinam V.S., Basheer M.G.S., Thayumanavan A., Murali K.R., Sanjeeviraja C., Swaminathan V. and Jayachandran M., Influence of thickness on the microstructural , optoelectronic and morphological properties of nanocrystalline ZnSe thin films. *Materials Science and Engineering B*, **171**, 93–98(2010). https://doi.org/10.1016/j.mseb.2010.03.079.

21. Miah A.H., Begum J., Regulatory E., Uddin J. and Momin A., Influence of thickness on the structural and optical properties of ZnSe thin films Influence of Thickness on the Structural and Optical Properties of ZnSe Thin Films. *Journal of Applied Science and Technology*, **7**(2) 27-32(2010).

22. Raghu P., Naveen C., Sanjeev G. and Mahesh H., Thickness Dependent Optical Properties of ZnSe Thin Films. *International Journal of Engineering Research & Technology*, **2**, 3568–3572 (2013)

23. Sofiienko A.O. and Degoda V.Y., X-ray induced conductivity of ZnSe sensors at high temperatures. *Radiation Measurements*, **47**, 27–29(2012). https://doi.org/https://doi.org/10.1016/j.radmeas.2011.08.017

24. Güllü H.H., Bayraklı Ö. and Parlak D.E.Y.M., Study on the electrical properties of ZnSe / Si heterojunction diode. J*ournal of Materials Science: Materials in Electronics*, **28**, 17806–17815 (2017). https://doi.org/10.1007/s10854-017-7721-9.

25. Kowalik R. and Fitzner K., Analysis of the mechanism for electrodeposition of the ZnSe phase on Cu substrate. *Journal of Electroanalytical Chemistry*, **633**, 78–84(2009). https://doi.org/10.1016/J.JELECHEM.2009.04.029

26. Murali K.R., Structural and electrical properties of brush plated ZnTe films. *Journal of Materials Science*, **50**, 1692–1695(2006). https://doi.org/10.1016/j.sse.2006.09.003.

27. Kim D., Park K., Lee S. and Yoo B., Electrochemical synthesis of ZnTe thin films from citrate bath and their electrical properties with incorporation of Cu. *Materials Chemistry and Physics*, **179**, 10–16(2016). https://doi.org/10.1016/j.matchemphys.2016.04.046.

28. Jiang Y., Kou H., Li J., Yu S., Du Y., Ye W. and Wang C., Synthesis of ZnTe dendrites on multi-walled carbon nanotubes / polyimide nanocomposite membrane by electrochemical atomic layer deposition and photoelectrical property research. *Journal of Solid State Chemistry*, **194**, 336–342(2012). https://doi.org/10.1016/j.jssc.2012.05.018.

29. Soonmin H., Activated Carbon and Metal Chalcogenide in Applied Materials Research. *Physical Science & Biophysics Journal*, **4** (2), 1-10(2020). ISSN: 2641-9165 https://doi.org/10.23880/psbj-16000146

30. Eessaa A.K., El-Shamy A.M. and Reda Y., Fabrication of commercial nanoporous alumina by low voltage anodizing. *Egyptian Journal of Chemistry*, **61**, 175–185(2018). https://doi.org/10.21608/EJCHEM.2017.2189.1175

31. Moharam M.M., Elsayed E.M., Nino J.C., Abou-shahba, R.M. and Rashad M.M., Potentiostatic deposition of Cu_2O fi lms as p-ype transparent conductors at room temperature. *Thin Solid Films*, **616**, 760–766(2016). https://doi.org/10.1016/j.tsf.2016.10.005.

32. Al-bataineh Q.M., Telfah M., Ahmad A.A., Alsaad A.M., Qattan I.A., Baaziz H., Charifi Z. and Telfah A.: Crystal Defects , Optical and Optoelectronic Properties of ZnO : CeO 2 Mixed Oxide Thin Films. *Photonics*, **7**, 1–19 (2020). https://doi.org/10.3390/photonics7040112.

33. Tabbakh A.A. Al, Crystallite size and lattice strain of lithiated spinel material for rechargeable battery by X □ ray diffraction peak □ broadening analysis. *international journal of energy research*, **43** (5), 1903–1911(2019). https://doi.org/10.1002/er.4390.

34. Shenouda A.Y.and Sayed E.S.M. El,

دراسات عن الترسيب الكهربائي لسيلينيد الزنك وتيلريد الزنك وسلوك الخلية الكهروكيميائية الضوئية

السيد مصطفي السيد [1]، عاطف يوسف شنوده[1]
قسم المعالجه الكيميائيه والكهربيه-مركز بحوث وتطوير الفلزات- القاهره- مصر

تم في هذا البحث دراسة الترسيب الكهربائي لمركبات سيلينيد الزنك ZnSe وتليريد الزنك ZnTeعلى مهابط من التيتانيوم ومهبط موصل زجاجي مصنوع من اوكسيد الانديم القصديري باستخدام تقنيه الفولتمامتريه الدائريه و بتقنيه الجهد الثابت مع الزمن كذلك تم تتبع تاثير السلوك الكهروكيميائي لتواجد أنواع أيونات الزنك والسيلينيوم والتيلريم و الموجوده بتركيزات مختلفه داخل حوض الترسيب باستخدام تقنيه وقياسات الفولتميتريه الدائريه ولوحظ الاتي حدث الترسيب الكهربي لسيلينيد الزنك عند جهد مهبطي ثابت مع الزمن قيمته -0.5 فولت بينما تم ترسيب تيليريد الزنك عند جهد مهبطي ثابت مع الزمن -0.7 فولت مقابل القطب الثابت عالميا من الزئبق وكبريتات الزئبيق. كشفت نتايج بيانات حيود أشعة السينيه عن قمم مميزة جدا لهيكل النظام المكعب لكل من تيليريد الزنك وسيلينيد الزنك مع مراحل هيكلية مكعبة بشكل جيد. تم تسجيل قيم مقياس الطيف الضوئي للمركبات المترسبه والتي رصدت ظهور حدوث حافة الإرسال لسيلينيد الزنك المترسب كهربيا عند 660 نانومتر بينما ظهرت حافه الارسال لمركب تيليريد الزنك المترسب كهربيا عند 750 نانومتر علي التوالي.
كذلك اظهرت النتايج المرصودة قيم طاقه فجوات لمركب سيلينيد الزنك عند 2.5 إلكترون فولت المترسب كهربيا وقيمه 2.27 الكترون فولت لمركب تيليريد الزنك المترسب كهربيا على التوالي.
أظهرت قيم أطياف المعاوقة الكهروكيميائية أن تيليريد الزنك المترسب كهربيا اكثر في قيم الموصليه الكهربيه و موصل أكثر من سيلينيد الزنك كذلك الحال في قيم كفاءات الخلايا الشمسية الكهروكيميائية الضوئية حيث انها كانت 5.1٪ لمركب سيلينيد الزنك كما كانت كفاءه الخلايا الشمسيه ٪ لمركب تيليريد الزنك 7.1 على التوالي.
من الناحيه الصناعيه يعتبر سيلينيد الزنك ZnSe وتليريد الزنك ZnTe بمثابة مادة بديلة صاعدة وواعده بدلاً من سيلينيد الكادميوم CdSe السام في الخلايا الضوئيه وتطبيقاتها كما ان هذان المركبان يحتويا على تطبيق واسع في صناعه اجهزه وأدوات مثل الثنائيات الباعثة للضوء الأزرق والصمامات الثنائية الضوئية والترانزستورات ذات الأغشية الرقيقة .

Electrodeposition, characterization and photo electrochemical properties of CdSe and CdTe. *Ain Shams Engineering Journal*, **6**, 341–346 (2015). https://doi.org/10.1016/j.asej.2014.07.010

35. Shenouda A.Y., Rashad M.M. and Chow L., Synthesis , characterization and performance of Cd 1 À x In x Te compound for solar cell applications. *Journal of Alloys and Compounds*, **563,** 39–43(2013). https://doi.org/10.1016/j.jallcom.2013.02.076.
36. Hassanien A.S. and Akl A.A., Superlattices and Microstructures Effect of Se addition on optical and electrical properties of chalcogenide CdSSe thin fi lms. *Superlattices and Microstructures.* **89**, 153–169(2016). https://doi.org/10.1016/j.spmi.2015.10.044.
37. Dhanasekaran V., Mahalingam T., Rhee J.K. and Chu J.P., Structural and optical properties of electrosynthesized ZnSe thin films. *International Journal for Light and Electron Optics (Optik)*. **124**, 255–260(2013). https://doi.org/10.1016/J.IJLEO.2011.11.063.
38. Gloeckler M., Sankin I. and Zhao Z., CdTe Solar Cells at the Threshold to 20 % Efficiency. *IEEE Journal of Photovoltaics*, **3**, 1389–1393(2013).https://doi.org/10.1109/JPHOTOV. 2013.2278661.